Investigation of Multi-Link Spatial Correlation Properties for Cooperative MIMO Channels

(Invited Paper)

Xiang Cheng[1,2], Cheng-Xiang Wang[3,4], Bo Ai[2], Xuefeng Yin[5], and Bingli Jiao[1]
[1]School of Electronics Engineering & Computer Science, Peking University, Beijing, 100871, China
[2]State Key Laboratory of Rail Traffic Control and Safety, Beijing Jiaotong University, Beijing 100044, China
[3]School of Information Science and Engineering, Shandong University, Shandong, China
[4]Joint Research Institute for Signal and Image Processing, Heriot-Watt University, Edinburgh EH14 4AS, UK
[5]School of Electronics and Information Engineering, Tongji University, Shanghai, China
Email: {xiangcheng, jiaobl}@pku.edu.cn, cheng-xiang.wang@hw.ac.uk, boai@bjtu.edu.cn, yinxuefeng@tongji.edu.cn

***Abstract*—In this paper, a comprehensive investigation of multi-link spatial correlation properties for cooperative multiple-input multiple-output (MIMO) wireless channels is presented. The impact of interested and important parameters, e.g., local scattering density (LSD) and environment-related parameters, on multi-link spatial correlation properties is completely investigated. Some interesting observations are found and useful conclusions are made. They are helpful for better understanding cooperative MIMO channels and for setting up more purposeful measurement campaigns.**

I. Introduction

Cooperative MIMO technology groups multiple radio devices to form virtual antenna arrays so that they can cooperate with each other by exploiting the spatial domain of mobile fading channels. Therefore, recently cooperative MIMO technology has been received much attention and employed in many new wireless systems, e.g., vehicular communication systems. As a new emerging technology, many research challenges in cooperative communications have to be addressed before its wide deployment. Among them, how to practically characterize cooperative MIMO channels is the fundamental one for the better design of cooperative MIMO systems [1].

Various statistical properties of cooperative MIMO channels for different scenarios have been investigated in many papers [2]– [5]. However, the investigation of multi-link correlation properties for cooperative MIMO channels is still in its infancy and more comprehensive study is needed for completely understanding cooperative MIMO channels.

In general, the multi-link spatial correlation consists of large scale fading multi-link spatial correlation and small scale fading multi-link spatial correlation. Compared with small scale fading multi-link spatial correlations, large scale fading multi-link spatial correlations have been widely investigated and standardized in many standard channel models, e.g., 3rd Generation Partnership Project (3GPP) Spatial Channel Model (SCM) [6], [7] and Wireless World Initiative New Radio Phase II (WINNER II) channel model [8]. Recently, a few papers [9]– [12] have studied the small scale fading multi-link spatial correlation and clearly shown its existence and importance. More recently, in [13], we have proposed a unified channel model framework for cooperative MIMO systems and preliminarily investigated small scale fading multi-link spatial correlations. The detailed and comprehensive investigation of multi-link spatial correlations is not the focus of this paper [13] and is lacking in the literature.

To fill the aforementioned gap, this paper first details the channel model proposed in [13] and highlights the physical meaning of key model parameters. Based on the developed channel model, the impact of key model parameters on multi-link spatial correlations will be comprehensively investigated and some interesting observations and useful conclusions will be given in this paper.

II. A GBSM for Cooperative MIMO Channels

In this section, the channel model first proposed in [13] will be introduced in more detailed and the physical meaning of key model parameters will be highlighted. Note that the introduced model in this section is a theoretical reference model rather than a simulation model [14]- [17].

The investigated scenario is a wideband cooperative relay communication environment that includes three different links: base station-relay station (BS-RS), RS-mobile station (MS), and BS-MS. Fig. 1 shows the geometry of the cooperative MIMO GBSM, combining the LoS components and scattered components. To keep the readability of Fig. 1, the LoS components are not shown. It is assumed that the BS, RS, and MS are all equipped with $A_B = A_R = A_M = 2$ uniform linear antenna arrays. The local scattering environment is characterized by the effective scatterers located on circular rings. Suppose there are N_1 effective scatterers around the MS lying on a circular ring of radius $R_{1n_1} \leq \xi_{n_1}^M \leq R_{1n_2}$ and the n_1th ($n_1 = 1, ..., N_1$) effective scatterer is denoted by S_{n_1}. Similarly, assume there are N_2 effective scatterers around the RS lying on a circular ring of radius $R_{2n_1} \leq \xi_{n_2}^R \leq R_{2n_2}$ and the n_2th ($n_2 = 1, ..., N_2$) effective scatterer is denoted by S_{n_2}. For the local scattering area around BS, N_3 effective scatterers lie on a circular ring of radius $R_{3n_1} \leq \xi_{n_3}^B \leq R_{3n_2}$ and the n_3th ($n_3 = 1, ..., N_3$) effective scatterer is denoted by S_{n_3}. The parameters in Fig. 1 are defined in Table I.

978-1-4673-5829-3/12/$26.00 ©2012 IEEE

In the following, we will show the channel gains of the three different links for the introduced cooperative MIMO GBSM.

A. BS-RS link

The channel gain of the BS-RS link between Antenna p_3 at the BS and Antenna p_2 at the RS can be expressed as

$$h_{p_3p_2} = h_{p_3p_2}^{LoS} + \sum_{i=1}^{3}\sum_{g=1}^{f_3(i)} h_{p_3p_2}^{ig} \tag{1}$$

where $h_{p_3p_2}^{LoS}$ denotes the LoS component and $h_{p_3p_2}^{ig}$ represents the gth i-bounced component with the following expressions

$$h_{p_3p_2}^{LoS} = \sqrt{\frac{K_{p_3p_2}\Omega_{p_3p_2}}{K_{p_3p_2}+1}} e^{-j2\pi\lambda^{-1}\chi_{p_3p_2}} \tag{2}$$

$$h_{p_3p_2}^{1g} = \sqrt{\frac{\eta_{p_3p_2}^{1g}\Omega_{p_3p_2}}{K_{p_3p_2}+1}} \lim_{N_g\to\infty} \sum_{n_g=1}^{N_g} \frac{1}{\sqrt{N_g}} e^{j\left(\psi_{n_g}-2\pi\lambda^{-1}\chi_{p_3p_2,n_g}\right)} \tag{3}$$

$$h_{p_3p_2}^{2g} = \sqrt{\frac{\eta_{p_3p_2}^{2g}\Omega_{p_3p_2}}{K_{p_3p_2}+1}} \lim_{N_{g1},N_{g2}\to\infty} \sum_{n_{g_1},n_{g_2}=1}^{N_{g_1},N_{g_2}} \frac{1}{\sqrt{N_{g_1}N_{g_2}}} \times e^{j\left(\psi_{n_{g_1},n_{g_2}}-2\pi\lambda^{-1}\chi_{p_3p_2,n_{g_1},n_{g_2}}\right)} \tag{4}$$

$$h_{p_3p_2}^{31} = \sqrt{\frac{\eta_{p_3p_2}^{31}\Omega_{p_3p_2}}{K_{p_3p_2}+1}} \lim_{N_1,N_2,N_3\to\infty} \sum_{n_1,n_2,n_3=1}^{N_1,N_2,N_3} \frac{1}{\sqrt{N_1N_2N_3}} \times e^{j\left(\psi_{n_1,n_2,n_3}-2\pi\lambda^{-1}\chi_{p_3p_2,n_1,n_2,n_3}\right)} \tag{5}$$

where g=1, 2, 3, $\{g_1, g_2\}$=$\{3, 2\}$ for g=1, $\{g_1, g_2\}$=$\{3, 1\}$ for g=2, and $\{g_1, g_2\}$=$\{1, 2\}$ for g=3. In (2)–(5), $\chi_{p_3p_2}$=$\varepsilon_{p_3p_2}$, $\chi_{p_3p_2,n_g}$=$\varepsilon_{p_3n_g}$+$\varepsilon_{n_gp_2}$, $\chi_{p_3p_2,n_{g_1},n_{g_2}}$=$\varepsilon_{p_3n_{g_1}}$+$\varepsilon_{n_{g_1}n_{g_2}}$+$\varepsilon_{n_{g_2}p_2}$, and $\chi_{p_3p_2,n_1,n_2,n_3}$=$\varepsilon_{p_3n_3}$+$\varepsilon_{n_3n_1}$+$\varepsilon_{n_1n_2}$+$\varepsilon_{n_2p_2}$ are the travel times of the waves through the link B_{p_3}–R_{p_2}, B_{p_3}–S_{n_g}–R_{p_2}, B_{p_3}–$S_{n_{g_1}}$–$S_{n_{g_2}}$–R_{p_2}, and B_{p_3}–S_{n_3}–S_{n_1}–S_{n_2}–R_{p_2}, respectively. The symbols $K_{p_3p_2}$ and $\Omega_{p_3p_2}$ designate the Ricean factor and the total power of the BS-RS link, respectively. Parameters $\eta_{p_3p_2}^{1g}$, $\eta_{p_3p_2}^{2g}$, and $\eta_{p_3p_2}^{31}$ specify how much the single-, double-, and triple-bounced rays contribute to the total scattered power $\Omega_{p_3p_2}/(K_{p_3p_2}+1)$ with $\sum_{g=1}^{3}(\eta_{p_3p_2}^{1g}+\eta_{p_3p_2}^{2g})+\eta_{p_3p_2}^{31}=1$. The phases ψ_{n_g}, $\psi_{n_{g_1},n_{g_2}}$, and ψ_{n_1,n_2,n_3} are i.i.d. random variables with uniform distributions over $[-\pi, \pi)$.

From Fig. 1 and based on the normally used assumption $\min\{D_1, D_2, D_3\} \gg \max\{\delta_1, \delta_2, \delta_3\}$ [18] and the application of the law of cosines in appropriate triangles, the distances $\varepsilon_{p_3p_2}$, $\varepsilon_{p_3n_g}$, $\varepsilon_{n_gp_2}$, $\varepsilon_{n_1n_2}$, $\varepsilon_{n_3n_2}$, and $\varepsilon_{n_3n_1}$ in (2)–(5) can be expressed as $\varepsilon_{p_3p_2} \approx D_3 - \frac{\delta_3}{2}\cos(\beta_3-\theta') + \frac{\delta_2}{2}\cos(\beta_2-\theta')$, $\varepsilon_{p_3n_g} \approx \xi_{n_g}^B - \frac{\delta_3}{2}\cos(\beta_3-\alpha_{1n_g})$, $\varepsilon_{n_gp_2} \approx \xi_{n_g}^R - \frac{\delta_2}{2}\cos(\beta_2-\alpha_{2n_g})$, $\varepsilon_{n_1n_2} = [(\xi_{n_1}^R)^2 + (\xi_{n_2}^R)^2 - 2\xi_{n_1}^R\xi_{n_2}^R\cos(\alpha_{2n_1}-\alpha_{2n_2})]^{1/2}$, and $\varepsilon_{n_3n_\varrho} = [(\xi_{n_3}^B)^2+(\xi_{n_\varrho}^B)^2-2\xi_{n_3}^B\xi_{n_\varrho}^B\cos(\alpha_{3n_3}-\alpha_{1n_\varrho})]^{1/2}$ where $\xi_{n_1}^B = (D_1^2+(\xi_{n_1}^M)^2+2D_1\xi_{n_1}^M\cos\alpha_{1n_1})^{1/2}$, $\xi_{n_1}^R = (D_2^2+(\xi_{n_1}^M)^2+2D_2\xi_{n_1}^M\cos(\alpha_{1n_1}+\theta))^{1/2}$, $\xi_{n_2}^B = (D_3^2+(\xi_{n_2}^R)^2+2D_3\xi_{n_2}^R\cos(\alpha_{2n_2}-\theta'))^{1/2}$, $\xi_{n_3}^R=(D_3^2+(\xi_{n_3}^B)^2-2D_3\xi_{n_3}^B\cos(\alpha_{3n_3}-\theta'))^{1/2}$, $\xi_{n_2}^R \in [R_{1n_2}, R_{2n_2}]$, $\xi_{n_3}^B \in [R_{1n_3}, R_{2n_3}]$, $\varrho = 1, 2$, and g=1, 2, 3. Note that the AoD α_{3n_1}, α_{3n_2}, α_{3n_3} and AoA α_{2n_1}, α_{2n_2}, α_{2n_3} are independent for double- and triple-bounced rays, while they are interdependent for single-bounced rays. It is worth highlighting that scatterers S_{n_g} around MS, RS, and BS are relevant to the angles α_{1n_1}, α_{2n_2}, and α_{3n_3}, respectively. Therefore, all other AoDs and AoAs have to be related to the aforementioned three key angles. By following the general method given in [18], the relationship of the key angles with other AoAs and AoDs of BS-RS link can be obtained as: $\sin\alpha_{3n_1} = \frac{\xi_{n_1}^M}{\xi_{n_1}^B}\sin\alpha_{1n_1}$, $\sin(\alpha_{2n_1}+\theta) = \frac{\xi_{n_1}^M}{\xi_{n_1}^R}\sin(\theta+\alpha_{1n_1})$, $\sin(\alpha_{3n_2}-\theta') = \frac{\xi_{n_2}^R}{\xi_{n_2}^B}\sin(\alpha_{2n_2}-\theta')$, and $\sin(\alpha_{2n_3}-\theta') = \frac{\xi_{n_3}^B}{\xi_{n_3}^R}\sin(\alpha_{3n_3}-\theta')$.

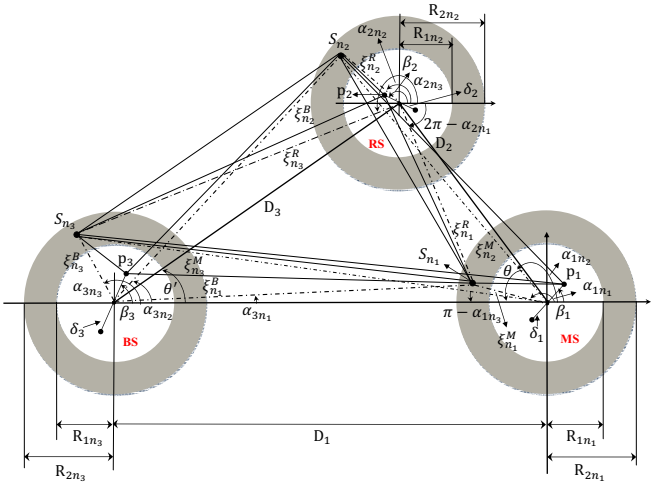

Fig. 1. The proposed cooperative MIMO GBSM.

TABLE I. DEFINITION OF PARAMETERS IN FIG. 2.

D_1, D_2, D_3	distances of BS-MS, RS-MS, and BS-RS, respectively
R_{1n_1}, R_{2n_1}; R_{1n_2}, R_{2n_2}; R_{1n_3}, R_{2n_3}	min and max radii of the circular rings around the MS, RS and BS, respectively
θ, θ'	angles between the RS-MS link and BS-MS link, and between the BS-RS link and BS-MS link, respectively
$\delta_1, \delta_2, \delta_3$	antenna element spacings of MS, RS and BS, respectively
$\beta_1, \beta_2, \beta_3$	orientations of the MS, RS and RS antenna arrays in the x-y plane (relative to the x-axis), respectively
$\alpha_{1n_i}, \alpha_{2n_i}$, and α_{3n_i}	azimuth angles of S_{n_i}-MS, S_{n_i}-RS, and S_{n_i}-BS links in the x-y plane (relative to the x-axis), respectively
$\xi_{n_1}^B, \xi_{n_2}^B, \xi_{n_3}^B$	distances d(BS,S_{n_1}), d(BS,S_{n_2}), and d(BS,S_{n_3}), respectively
$\xi_{n_1}^R, \xi_{n_2}^R, \xi_{n_3}^R$	distances d(RS,S_{n_1}), d(RS,S_{n_2}), and d(RS,S_{n_3}), respectively
$\xi_{n_1}^M, \xi_{n_2}^M, \xi_{n_3}^M$	distances d(MS,S_{n_1}), d(MS,S_{n_2}), and d(MS,S_{n_3}), respectively
$\varepsilon_{p_in_g}(\varepsilon_{n_gp_i})$, $\varepsilon_{p_ip_j}$, and $\varepsilon_{n_gn_k}$	distances $d(p_i, S_{n_g})$, $d(p_i, p_j)$, and $d(S_{n_g}, S_{n_k})$, respectively

B. BS-MS link

The channel gain of BS-MS link between antenna p_3 at BS and antenna p_1 at MS can be expressed as

$$h_{p_3p_1} = h_{p_3p_1}^{LoS} + \sum_{i=1}^{3}\sum_{g=1}^{f_3(i)} h_{p_3p_1}^{ig} \tag{6}$$

where $h_{p_3p_1}^{LoS}$ denotes the LoS component and $h_{p_3p_1}^{ig}$ represents the gth i-bounced component with the following expressions

$$h_{p_3p_1}^{LoS} = \sqrt{\frac{K_{p_3p_1}\Omega_{p_3p_1}}{K_{p_3p_1}+1}} e^{-j2\pi\lambda^{-1}\chi_{p_3p_1}} \tag{7}$$

$$h_{p_3p_1}^{1g} = \sqrt{\frac{\eta_{p_3p_1}^{1g}\Omega_{p_3p_1}}{K_{p_3p_1}+1}} \lim_{N_g\to\infty} \sum_{n_g=1}^{N_g} \frac{1}{\sqrt{N_g}} e^{j\left(\psi_{n_g}-2\pi\lambda^{-1}\chi_{p_3p_1,n_g}\right)} \tag{8}$$

$$h_{p_3p_1}^{2g} = \sqrt{\frac{\eta_{p_3p_1}^{2g}\Omega_{p_3p_1}}{K_{p_3p_1}+1}} \lim_{N_{g_1},N_{g_2}\to\infty} \sum_{n_{g_1},n_{g_2}=1}^{N_{g_1},N_{g_2}} \frac{1}{\sqrt{N_{g_1}N_{g_2}}} \times e^{j\left(\psi_{n_{g_1},n_{g_2}}-2\pi\lambda^{-1}\chi_{p_3p_1,n_{g_1},n_{g_2}}\right)} \tag{9}$$

$$h_{p_3p_1}^{31} = \sqrt{\frac{\eta_{p_3p_1}^{31}\Omega_{p_3p_1}}{K_{p_3p_1}+1}} \lim_{N_1,N_2,N_3\to\infty} \sum_{n_1,n_2,n_3=1}^{N_1,N_2,N_3} \frac{1}{\sqrt{N_1N_2N_3}} \times e^{j\left(\psi_{n_1,n_2,n_3}-2\pi\lambda^{-1}\chi_{p_3p_1,n_1,n_2,n_3}\right)} \tag{10}$$

where parameters g, g_1, and g_2 are the same as the ones in (2)–(5). In (7)–(10), $\chi_{p_3p_1}=\varepsilon_{p_3p_1}$, $\chi_{p_3p_1,n_g}=\varepsilon_{p_3n_g}+\varepsilon_{n_gp_1}$, $\chi_{p_3p_1,n_{g_1},n_{g_2}}=\varepsilon_{p_3n_{g_1}}+\varepsilon_{n_{g_1}n_{g_2}}+\varepsilon_{n_{g_2}p_1}$, and $\chi_{p_3p_1,n_1,n_2,n_3}=\varepsilon_{p_3n_3}+\varepsilon_{n_3n_2}+\varepsilon_{n_2n_1}+\varepsilon_{n_1p_1}$ are the travel times of the waves through the link B_{p_3}–M_{p_1}, B_{p_3}–S_{n_g}–M_{p_1}, B_{p_3}–$S_{n_{g_1}}$–$S_{n_{g_2}}$–M_{p_1}, and $B_{p_3}-S_{n_3}-S_{n_2}-S_{n_1}-M_{p_1}$, respectively. The symbols $K_{p_3p_1}$ and $\Omega_{p_3p_1}$ designate the Ricean factor and the total power of the BS-MS link, respectively. Parameters $\eta_{p_3p_1}^{1g}$, $\eta_{p_3p_1}^{2g}$, and $\eta_{p_3p_1}^{31}$ specify how much the single-, double-, and triple-bounced rays contribute to the total scattered power $\Omega_{p_3p_1}/(K_{p_3p_1}+1)$ with $\sum_{g=1}^{3}(\eta_{p_3p_1}^{1g}+\eta_{p_3p_1}^{2g})+\eta_{p_3p_1}^{31}=1$. The phases ψ_{n_1,n_3} is i.i.d. random variable with uniform distributions over $[-\pi,\pi)$.

Similar to the BS-RS link, by applying of the law of cosines in appropriate triangles, with the help of the normally used assumption $\min\{D_1,D_2,D_3\} \gg \max\{\delta_1\delta_2,\delta_3\}$, we have the following expressions of the desired distances as $\varepsilon_{p_3p_1} \approx D_1-\frac{\delta_3}{2}\cos\beta_3+\frac{\delta_1}{2}\cos(\beta_1)$ and $\varepsilon_{n_gp_1} \approx \xi_{n_g}^M-\frac{\delta_1}{2}\cos(\beta_1-\phi_{n_g})$ where g=1, 2, 3, $\xi_{n_1}^M\in[R_{1n_1},R_{2n_1}]$, $\xi_{n_2}^M=\sqrt{D_2^2+(\xi_{n_2}^R)^2-2D_2\xi_{n_2}^R\cos\varphi_{n_2}}$ with $\varphi_{n_2}=2\pi-\theta'-\alpha_{2n_2}$, and $\xi_{n_3}^M=\sqrt{D_1^2+(\xi_{n_3}^B)^2-2D_1\xi_{n_3}^B\cos\alpha_{3n_3}}$. The expressions of other interested distances $\varepsilon_{p_3n_1}$, $\varepsilon_{p_3n_2}$, $\varepsilon_{p_3n_3}$, $\varepsilon_{n_3n_1}$, $\varepsilon_{n_3n_2}$, and $\varepsilon_{n_2n_1}=\varepsilon_{n_1n_2}$ have been given previously in the BS-RS link. Similar to the BS-RS link, angles α_{1n_2} and α_{1n_3} need to be related to any one of three key angles as $\sin(\alpha_{1n_2}+\theta)=\frac{\xi_{n_2}^R}{\xi_{n_2}^M}\sin(\alpha_{2n_2}+\theta)$ and $\sin\alpha_{1n_3}=\frac{\xi_{n_3}^B}{\xi_{n_3}^M}\sin\alpha_{3n_3}$.

Similar to the BS-RS link, the above derived expressions of the distances and angles are applicable to various basic scenarios. For outdoor macro-cell and micro-cell scenarios, by using the assumption $\min\{D_1,D_2,D_3\}\gg\max\{\xi_{n_1}^M,\xi_{n_2}^R,\xi_{n_3}^B\}$, the following reduced expressions can be obtained as: $\xi_{n_2}^M\approx D_2-\xi_{n_2}^R\cos\varphi_{n_2}$ with $\varphi_{n_2}=2\pi-(\alpha_{2n_2}+\theta)$, $\xi_{n_3}^M\approx D_1-\xi_{n_3}^B\cos\alpha_{3n_3}$, $\alpha_{1n_2}\approx\pi-\theta-\frac{\xi_{n_2}^R}{D_2}\sin(\theta+\alpha_{2n_2})$, and $\alpha_{1n_3}\approx\pi-\frac{\xi_{n_3}^B}{D_1}\sin\alpha_{3n_3}$.

C. RS-MS link

The channel gain of RS-MS link between antenna p_2 at BS and antenna p_1 at MS can be expressed as

$$h_{p_2p_1} = h_{p_2p_1}^{LoS} + \sum_{i=1}^{3}\sum_{g=1}^{f_3(i)} h_{p_2p_1}^{ig} \tag{11}$$

where $h_{p_2p_1}^{LoS}$ denotes the LoS component and $h_{p_2p_1}^{ig}$ represents the gth i-bounced component with the following expressions

$$h_{p_2p_1}^{LoS} = \sqrt{\frac{K_{p_2p_1}\Omega_{p_2p_1}}{K_{p_2p_1}+1}} e^{-j2\pi\lambda^{-1}\chi_{p_2p_1}} \tag{12}$$

$$h_{p_2p_1}^{1g} = \sqrt{\frac{\eta_{p_2p_1}^{1g}\Omega_{p_2p_1}}{K_{p_2p_1}+1}} \lim_{N_g\to\infty} \sum_{n_g=1}^{N_g} \frac{1}{\sqrt{N_g}} e^{j\left(\psi_{n_g}-2\pi\lambda^{-1}\chi_{p_2p_1,n_g}\right)} \tag{13}$$

$$h_{p_2p_1}^{2g} = \sqrt{\frac{\eta_{p_2p_1}^{2g}\Omega_{p_2p_1}}{K_{p_2p_1}+1}} \lim_{N_{g_1},N_{g_2}\to\infty} \sum_{n_{g_1},n_{g_2}=1}^{N_{g_1},N_{g_2}} \frac{1}{\sqrt{N_{g_1}N_{g_2}}} \times e^{j\left(\psi_{n_{g_1},n_{g_2}}-2\pi\lambda^{-1}\chi_{p_2p_1,n_{g_1},n_{g_2}}\right)} \tag{14}$$

$$h_{p_2p_1}^{31} = \sqrt{\frac{\eta_{p_2p_1}^{31}\Omega_{p_2p_1}}{K_{p_2p_1}+1}} \lim_{N_1,N_2,N_3\to\infty} \sum_{n_1,n_2,n_3=1}^{N_1,N_2,N_3} \frac{1}{\sqrt{N_1N_2N_3}} \times e^{j\left(\psi_{n_1,n_2,n_3}-2\pi\lambda^{-1}\chi_{p_2p_1,n_1,n_2,n_3}\right)} \tag{15}$$

where parameters g, g_1, and g_2 are the same as the ones in (2)–(5). In (12)–(15), $\chi_{p_2p_1}=\varepsilon_{p_2p_1}$, $\chi_{p_2p_1,n_g}=\varepsilon_{p_2n_g}+\varepsilon_{n_gp_1}$, $\chi_{p_2p_1,n_{g_1},n_{g_2}}=\varepsilon_{p_2n_{g_1}}+\varepsilon_{n_{g_1}n_{g_2}}+\varepsilon_{n_{g_2}p_1}$, and $\chi_{p_2p_1,n_1,n_2,n_3}=\varepsilon_{p_2n_2}+\varepsilon_{n_2n_3}+\varepsilon_{n_3n_1}+\varepsilon_{n_1p_1}$ are the travel times of the waves through the link R_{p_2}–M_{p_1}, R_{p_2}–S_{n_g}–M_{p_1}, R_{p_2}–$S_{n_{g_1}}$–$S_{n_{g_2}}$–M_{p_1}, and $R_{p_2}-S^{(n_2)}-S^{(n_3)}-S^{(n_1)}-M_{p_1}$, respectively. The symbols $K_{p_2p_1}$ and $\Omega_{p_2p_1}$ designate the Ricean factor and the total power of the RS-MS link, respectively. Parameters $\eta_{p_2p_1}^{1g}$, $\eta_{p_2p_1}^{2g}$, and $\eta_{p_2p_1}^{31}$ specify how much the single-, double-, and triple-bounced rays contribute to the total scattered power $\Omega_{p_2p_1}/(K_{p_2p_1}+1)$ with $\sum_{g=1}^{3}(\eta_{p_2p_1}^{1g}+\eta_{p_2p_1}^{2g})+\eta_{p_2p_1}^{31}=1$.

From Fig. 1, it is clear that all the expressions of the desired distances have been given previously in BS-RS and BS-MS links except the distance $\varepsilon_{p_2p_1}$ with the following expression $\varepsilon_{p_2p_1} \approx D_2-\frac{\delta_2}{2}\cos(\beta_2+\theta)-\frac{\delta_1}{2}\cos(\beta_1-\theta)$ where the assumption $D_2\gg\max\{\delta_2,\delta_1\}$ is utilized.

In the literature, different scatterer distributions have been proposed to characterize the key angles α_{1n_1}, α_{2n_2}, and α_{3n_3}, such as the uniform, Gaussian, wrapped Gaussian, and cardioid PDFs [19]. In this paper, the von Mises PDF [21] is used, which is more generic and can approximate all the aforementioned PDFs [18]. The von Mises PDF is defined as $f(\phi)\triangleq\exp[k\cos(\phi-\mu)]/[2\pi I_0(k)]$, where $\phi\in[-\pi,\pi)$, $I_0(\cdot)$ is the zeroth-order modified Bessel function of the first kind, $\mu\in[-\pi,\pi)$ accounts for the mean value of the angle ϕ, and k ($k\geq0$) is a real-valued parameter that controls the angle spread of the angle ϕ. In this paper, for the key angles, i.e., the α_{1n_1}, α_{2n_2}, and α_{3n_3}, we use appropriate parameters (μ and k) of the von Mises PDF as μ_1 and k_1, μ_2 and k_2, and μ_3 and k_3, respectively.

D. Key Model Parameters

In [13], how to adjust key model parameters to make th GBSM adaptable to different cooperative scenarios has bee clearly addressed. In this section, we will focus on highlightin the physical meaning of key model parameters, which wi be useful for the investigation of the impact of these ke model parameters on multi-link spatial correlations in the nex section.

The main features of the introduced MIMO GBSM ar summarized in Table II. By properly adjusting the key mode parameters, the GBSM is suitable for 12 cooperative scenarios As shown in Table II, the key model parameters are th number of local scattering environment I, Ricean factors $K_{p_3p_2}$, $K_{p_3p_1}$, $K_{p_2p_1}$, and energy-related parameters $\eta^{ig}_{p_3p_2}$, $\eta^{ig}_{p_3p_1}$, and $\eta^{ig}_{p_2p_1}$. The parameter setting of I is basically based on basic scenario. For outdoor micro-cell, pico-cell, and indoor scenarios, we assume that the BS, RS, and MS are all surrounded by local scattering area as shown in Fig. 2 and thus $I = 3$ in this case. For outdoor Marco-cell scenario, the BS is free of scatterers and thus $I = 2$. For outdoor macro-cell BS cooperation scenario, RS actually represents the other BS, symbolled as BS2, and thus is free of scatterers as well. In this case, we have the currently most mature cooperative MIMO scheme: CoMP and the number of local scattering area $I = 1$. The energy-related parameters specify how much the different rays contribute to the total scattered power. Therefore, the energy-related parameters determine the contribution of scattered rays to the received power.

In general, the longer distance of the link and/or the higher

TABLE II. MAIN FEATURES OF THE COOPERATIVE MIMO GBSM.

<table>
<tr><td colspan="4">The Cooperative MIMO GBSM</td></tr>
<tr><td>Links</td><td colspan="3">Three different links: BS-RS, RS-MS, and BS-MS links. (can be easily extended to include more links)</td></tr>
<tr><td rowspan="3">Scenarios</td><td colspan="3">12 cooperative scenarios</td></tr>
<tr><td colspan="2">Physical scenarios</td><td>Application scenarios</td></tr>
<tr><td colspan="2">Outdoor Macro-cell
Outdoor Micro-cell
Outdoor Pico-cell
Indoor scenarios</td><td>BS cooperation
MS cooperation
Relay cooperation</td></tr>
<tr><td rowspan="3">Key Parameters</td><td>I</td><td>$k_{p_3p_2}$
$k_{p_3p_1}$
$k_{p_2p_1}$</td><td>$\eta^{1g}_{p_3p_2/p_3p_1/p_2p_1}$
$\eta^{2g}_{p_3p_2/p_3p_1/p_2p_1}$
$\eta^{31}_{p_3p_2/p_3p_1/p_2p_1}$
$(g = 1, 2, 3)$</td></tr>
<tr><td>The number of local scattering areas.</td><td>Ricean factor of the BS-RS link, BS-MS link, and RS-MS link, respectively.</td><td>Energy-related parameters that specify how much the single-, double- and triple-bounced rays contribute to the total scattered power of the BS -RS/BS-MS/ RS-MS link, respectively.</td></tr>
<tr><td colspan="3">By properly adjusting the key parameters, the proposed cooperative MIMO GBSM is suitable for 12 cooperation scenarios.</td></tr>
</table>

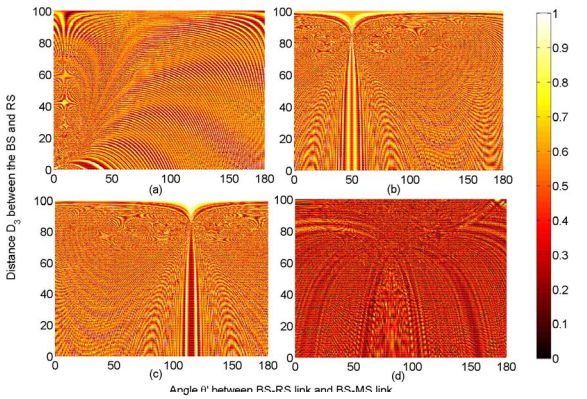

Fig. 2. Absolute values of spatial correlation functions between the BS-RS link and BS-MS link for (a) the first single-bounced component $\rho^{11}_{p_3p_2,p'_3p_1}$; (b) the third single-bounced component $\rho^{13}_{p_3p_2,p'_3p_1}$; (c) the third double-bounced component $\rho^{23}_{p_3p_2,p'_3p_1}$; and (d) the triple-bounced component $\rho^{31}_{p_3p_2,p'_3p_1}$.

the local scattering density (LSD), the smaller the Ricean factors and the larger the energy-related parameters of multi-bounced components, i.e., the multi-bounced components bear more energy than single-bounced components. Since the local scattering area is highly related to the degree of link heterogeneity in cooperative MIMO systems as presented in [10], [20], the LSD significantly affects the channel characteristics and should be investigated. In general, the higher the LSD, the lower the possibility that the devices (BS/MS/RS) share the same scatterers. In this case, the cooperative MIMO environments present lower environment similarity. Therefore, the higher the LSD, the lower the environment similarity.

E. Multi-Link Spatial Correlations

Based on the introduced cooperative MIMO GBSM, the multi-link spatial correlation functions can be derived for non-isotropic scattering cooperative MIMO environments. The normalized spatial correlation function between any two links characterized by channel gains h_{pq} and $h_{p'q'}$, respectively, is defined as [19]

$$\rho_{pq,p'q'} = \frac{\mathbf{E}\left[h_{pq}h^*_{p'q'}\right]}{\sqrt{\Omega_{pq}\Omega_{p'q'}}} \tag{16}$$

where $(\cdot)^*$ denotes the complex conjugate operation, $\mathbf{E}[\cdot]$ is the statistical expectation operator, $p, p' \in \{1, 2, ..., M_T\}$, and $q, q' \in \{1, 2, ..., M_R\}$. Substituting corresponding channel gains given in Sections II-A, B, and C into (16), we can have the correlation function between any two links as the expressions shown in [13] and thus omitted here for brevity.

III. NUMERICAL RESULTS AND ANALYSIS

In this section, the interested multi-link spatial correlations will be numerically analyzed in detail. Without loss of generality, the spatial correlation properties between the BS-RS link and BS-MS link are chosen for further investigation. The parameters for the following numerical results are listed here

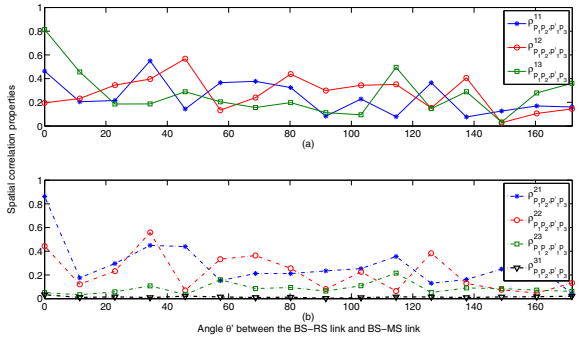

Fig. 3. Absolute values of spatial correlation functions between the BS-RS link and BS-MS link for (a) the single-bounced components and (b) the double- and triple-bounce components.

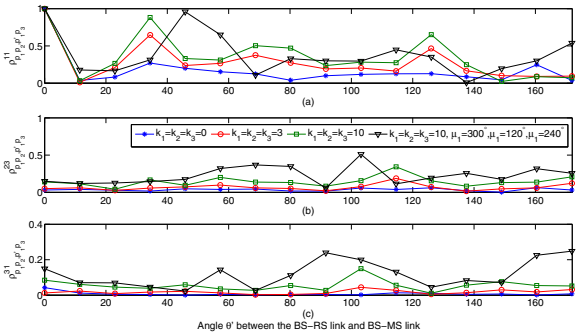

Fig. 4. Absolute values of spatial correlation functions between the BS-RS link and BS-MS link for (a) the first single-bounced component $\rho^{11}_{p_3p_2,p'_3p_1}$; (b) the third double-bounced component $\rho^{23}_{p_3p_2,p'_3p_1}$; and (c) the triple-bounced component $\rho^{31}_{p_3p_2,p'_3p_1}$ with different values of parameters k_g and μ_g $(g = 1, 2, 3)$.

or specified otherwise: $f = 2.4$GHz, $D_1 = D_3 = 100$m, $R_{1n_1} = R_{1n_2} = R_{1n_3} = 5$m, $R_{2n_1} = R_{2n_2} = R_{2n_3} = 50$m, $\delta_3 = \delta_2 = \delta_1 = 0$, $\beta_3 = 30°$, $\beta_2 = \beta_1 = 60°$, $K_{p_3p_2} = K_{p'_3p_1} = 0$, $k_1 = k_2 = k_3 = 10$, $\mu_1 = 120°$, $\mu_2 = 300°$, and $\mu_3 = 60°$.

A. Impact of Key Parameters on Multi-Link Spatial Correlation

Fig. 2 illustrates the spatial correlation properties of different components in (27) as a function of θ' and D_3. It is obvious that high spatial correlations between the BS-RS link and BS-MS link can occur at certain distances D_3 and certain values of angle θ' for different components. This again demonstrates that small scale spatial fading correlation should not be simply neglected as addressed in [9] and also highlights the importance of the work presented in this paper.

In Fig. 3, we present the spatial correlation properties of all scattered components in (27) with parameters $\delta_3 = \delta_2 = \delta_1 = 3\lambda$ and $k_1 = k_2 = k_3 = 3$. Fig. 3 clearly depicts that the spatial correlation properties vary significantly for different scattered components. More importantly, we notice that the scattered component that includes more bounced rays

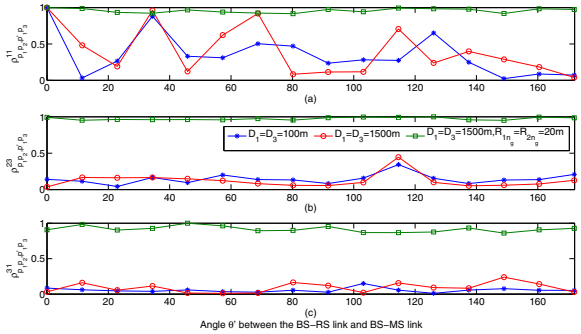

Fig. 5. Absolute values of spatial correlation functions between the BS-RS link and BS-MS link for (a) the first single-bounced component $\rho^{11}_{p_3p_2,p'_3p_1}$; (b) the third double-bounced component $\rho^{23}_{p_3p_2,p'_3p_1}$; and (c) the triple-bounced component $\rho^{31}_{p_3p_2,p'_3p_1}$ with different values of parameters D_3, R_{1n_g}, and R_{2n_g} $(g = 1, 2, 3)$.

expresses lower spatial correlation properties. This is because with more bounced rays, the component is related to more local scattering areas and thus easier experiences higher degree of link heterogeneity, resulting in lower link similarity for this component.

Figs. 4 and 5 compare the spatial correlation properties of different scattered components for different values of environment parameters D_g, R_{1n_g}, R_{2n_g}, k_g, and μ_g with $g = 1, 2, 3$. These environment parameters determine the distance among BS, RS, and MS, and decide the size and distribution of local scattering areas. It is clear that these environment parameters significantly affect the spatial correlation properties of different scattered components. From Fig. 4, we also observe that the increase of value k_g will enhance the spatial correlation. With larger value of k_g, the scatterers in local scattering area are more concentrated and the received power mainly comes from certain direction determined by μ_g. Therefore, in this case, the spatial correlation tends to be larger, which also agrees with the conclusion in [11]. Fig. 5 also shows that the local scattering area with smaller size leads to higher spatial correlation properties. Compared to the local scattering area with larger size, the local scattering area with smaller size means the effective scatterers are more concentrated and thus results in higher spatial correlation properties. It also allows us to conclude that compared to a narrowband cooperative MIMO system, a wideband system has a high possibility to express lower spatial correlation properties as the wider the system band, the more likely the system experiences local scattering areas with larger size.

In Fig. 6, the comparison of spatial correlation properties of different scattered components for different values of antenna element spacing δ_g and antenna array tilt angles β_g with $g = 1, 2, 3$ and parameters $k_1 = k_2 = k_3 = 3$ is presented. It is shown that both antenna element spacing and antenna array tilt angle affect the spatial correlation properties of different scattered components and the increase of antenna spacing δ_g will decrease spatial correlations. However, the impact of

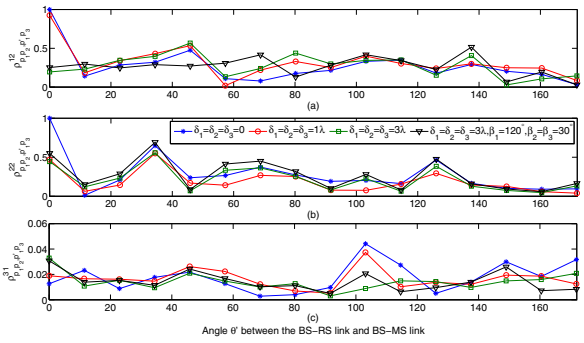

Fig. 6. Absolute values of spatial correlation functions between the BS-RS link and BS-MS link for (a) the second single-bounced component $\rho^{12}_{p_3p_2,p'_3p_1}$; (b) the second double-bounced component $\rho^{22}_{p_3p_2,p'_3p_1}$; and (c) the triple-bounced component $\rho^{31}_{p_3p_2,p'_3p_1}$ with different values of parameters δ_g and β_g $(g = 1, 2, 3)$.

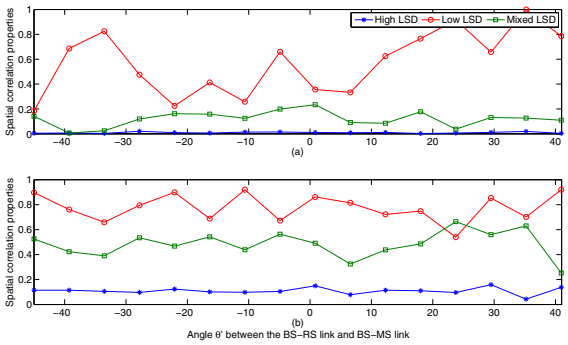

Fig. 7. Absolute values of spatial correlation functions between the BS-RS link and BS-MS link for (a) the outdoor macro-cell MS cooperation scenario and (b) the indoor MS cooperation scenario with different LSDs.

parameters δ_g and β_g on spatial correlation properties tends to be marginal for the scattered components with more bounced rays.

B. Validation of the Introduced Cooperative MIMO GBSM

So far, based on Figs. 2–6 we have investigated in more detail the spatial correlation properties of different scattered components separately. In general, we find that the multi-link spatial correlation increases with the increase of the environment parameter k_g, with the decrease of the size of local scattering area, with the decrease of the value i for a i-bounced rays, and/or with the decrease of the antenna spacing δ_g. According to the above obtained observation and conclusions, we will investigate the spatial correlation properties of the proposed cooperative MIMO GBSM in (16) and thus validate the utility of the proposed cooperative MIMO channel model. Without loss of any generality, the outdoor macro-cell MS cooperation scenario and indoor MS cooperation scenario are chosen for further investigation. As shown in Fig. 8, three different LSD conditions are considered with parameters $\delta_3 = \delta_2 = \delta_1 = 3\lambda$, i.e., high LSD, low LSD, and mixed LSD.

For outdoor macro-cell MS cooperation scenario, as mentioned in Section III, the BS is free of scatterers and the RS actually represents the other MS, symbolled as MS2. Therefore, we have the energy-related parameters related to the local scatterers around BS to be equal to zero, i.e., $\eta^{13}_{p_3p_2} = \eta^{13}_{p'_3p_1} = \eta^{21}_{p_3p_2} = \eta^{21}_{p'_3p_1} = \eta^{22}_{p_3p_2} = \eta^{22}_{p'_3p_1} = \eta^{31}_{p_3p_2} = \eta^{31}_{p'_3p_1} = 0$, and assume $D_1 = D_3 = 1500$m and $K_{p_3p_2} = K_{p'_3p_1} = 0$ due to the large distance among BS, MS, and MS2. Considering the basic criterion of setting key model parameters expressed in Section III, we choose the other energy-related parameters as: $\eta^{11}_{p_3p_2} = \eta^{11}_{p'_3p_1} = \eta^{12}_{p_3p_2} = \eta^{12}_{p'_3p_1} = 0.05$ and $\eta^{23}_{p_3p_2} = \eta^{23}_{p'_3p_1} = 0.9$ for high LSD, and $\eta^{11}_{p_3p_2} = \eta^{11}_{p'_3p_1} = \eta^{12}_{p_3p_2} = \eta^{12}_{p'_3p_1} = 0.2$ and $\eta^{23}_{p_3p_2} = \eta^{23}_{p'_3p_1} = 0.6$ for low LSD. While for mixed LSD case, we consider the scenario that the local scattering area around MS presents low LSD and the one around MS2 shows high LSD, and thus assume the energy-related parameters as: $\eta^{11}_{p'_3p_1} = \eta^{12}_{p'_3p_1} = 0.2$, $\eta^{23}_{p'_3p_1} = 0.6$, $\eta^{11}_{p_3p_2} = \eta^{12}_{p_3p_2} = 0.1$, and $\eta^{23}_{p_3p_2} = 0.8$. In general, the higher the LSD, the more distributed and larger size the local scattering area, and thereby the smaller the value of k_g and the larger the value of $R_{2n_g} - R_{1n_g}$ $(g = 1, 2, 3)$. Therefore, we have the following environment parameters as: $k_1 = k_2 = 1$, $R_{1n_1} = R_{1n_2} = 5$m, and $R_{2n_1} = R_{2n_2} = 200$m for high LSD; $k_1 = k_2 = 10$, $R_{1n_1} = R_{1n_2} = 5$m, and $R_{2n_1} = R_{2n_2} = 20$m for low LSD; and $k_1 = 10$, $k_2 = 2$, $\mu_1 = 60°$, $\mu_2 = 120°$, $R_{1n_1} = R_{1n_2} = 5$m, $R_{2n_1} = 20$m, and $R_{2n_2} = 100$m for mixed LSD.

Similarly, for indoor MS cooperation scenario, the RS actually represents the other MS, symbolled as MS2. Considering the small distance among BS, MS, and MS2, we assume $D_1 = D_3 = 50$ m. For mixed LSD case, we consider the scenario that the local scattering areas around BS and MS present low LSDs and the one around MS2 shows high LSD. The key model parameters are chosen as follows: $K_{p_3p_2} = K_{p'_3p_1} = 0.1$, $\eta^{11}_{p_3p_2} = \eta^{11}_{p'_3p_1} = \eta^{12}_{p_3p_2} = \eta^{12}_{p'_3p_1} = \eta^{13}_{p_3p_2} = \eta^{13}_{p'_3p_1} = 0.05$, $\eta^{21}_{p_3p_2} = \eta^{21}_{p'_3p_1} = \eta^{22}_{p_3p_2} = \eta^{22}_{p'_3p_1} = \eta^{23}_{p_3p_2} = \eta^{23}_{p'_3p_1} = 0.2$, and $\eta^{31}_{p_3p_2} = \eta^{31}_{p'_3p_1} = 0.25$ for high LSD; $K_{p_3p_2} = K_{p'_3p_1} = 3$, $\eta^{11}_{p_3p_2} = \eta^{11}_{p'_3p_1} = \eta^{12}_{p_3p_2} = \eta^{12}_{p'_3p_1} = \eta^{13}_{p_3p_2} = \eta^{13}_{p'_3p_1} = 0.3$, and $\eta^{21}_{p_3p_2} = \eta^{21}_{p'_3p_1} = \eta^{22}_{p_3p_2} = \eta^{22}_{p'_3p_1} = \eta^{23}_{p_3p_2} = \eta^{23}_{p'_3p_1} = \eta^{31}_{p_3p_2} = \eta^{31}_{p'_3p_1} = 0.025$ for low LSD; and $K_{p_3p_2} = 0.5$, $K_{p'_3p_1} = 2.5$, $\eta^{11}_{p'_3p_1} = \eta^{12}_{p'_3p_1} = \eta^{13}_{p'_3p_1} = 0.25$, $\eta^{21}_{p'_3p_1} = 0.1$, $\eta^{22}_{p'_3p_1} = \eta^{23}_{p'_3p_1} = \eta^{31}_{p'_3p_1} = 0.05$, $\eta^{11}_{p_3p_2} = \eta^{12}_{p_3p_2} = \eta^{13}_{p_3p_2} = 0.05$, $\eta^{21}_{p_3p_2} = \eta^{23}_{p_3p_2} = 0.3$, $\eta^{22}_{p_3p_2} = 0.1$, and $\eta^{31}_{p_3p_2} = 0.15$ for mixed LSD. The following environment parameters are selected as: $k_1 = k_2 = k_3 = 1$, $R_{1n_1} = R_{1n_2} = R_{1n_3} = 2$m, and $R_{2n_1} = R_{2n_2} = R_{2n_3} = 25$m for high LSD; $k_1 = k_2 = k_3 = 10$, $R_{1n_1} = R_{1n_2} = R_{1n_3} = 2$m, and $R_{2n_1} = R_{2n_2} = R_{2n_3} = 8$m for low LSD; and $k_1 = 6$, $k_2 = 2$, $k_3 = 15$, $\mu_1 = 60°$, $\mu_2 = 120°$, $\mu_3 = 240°$, $R_{1n_1} = R_{1n_2} = R_{1n_3} = 2$m, $R_{2n_1} = 12$m, $R_{2n_2} = 20$m, and $R_{2n_3} = 5$m for mixed LSD.

Fig. 7 clearly shows that the LSD significantly affects the spatial correlation properties. It is observed that the higher

the LSD, the lower the spatial correlation properties. This is because that with a higher LSD, the local scattering area is more distributed and presents larger size, resulting in the received power comes from many different directions. Fig. 7 also illustrates that the indoor MS cooperation scenario has larger spatial correlation properties than the outdoor macro-cell MS cooperation scenario. This is basically resulted from the appearance of a LoS component in the indoor MS cooperation scenario due to the smaller distance among BS, MS, and MS2. Therefore, we can conclude that a high multi-link spatial correlation normally appears in a scenario with lower LSDs and LoS components. More importantly, from the observation in Fig. 3 and based on the constraints of the energy-related parameters for cooperative scenarios with different LSDs, we know that with a higher LSD, the multi-bounced components bear more energy than single-bounced components and thus the corresponding cooperative environment has a higher possibility to reveal a high degree of link heterogeneity, i.e., a low degree of environment similarity. Therefore, the above conclusion based on Fig. 7 is consistent with our intuition that a low degree of environment similarity results in low multi-link spatial correlations.

IV. Conclusions

This paper has comprehensively investigated multi-link spatial correlation properties for cooperative MIMO channels via a complete study of the impact of interesting and important parameters on these multi-link spatial correlations. Numerical results have shown that the antenna element spacings, environment parameters, and LSD have great impacts on multi-link spatial correlation properties. It has also been demonstrated that a high multi-link spatial correlation may exist if a cooperative communication system has a relatively narrow bandwidth and the underlying propagation environments have low LSDs and LoS components.

Acknowledgement

This work was jointly supported by the National Natural Science Foundation of China (Grant no. 61101079, 61210002, and 61222105), the Science Foundation for the Youth Scholar of Ministry of Education of China (Grant no. 20110001120129), the State Key Laboratory of Rail Traffic Control and Safety (RCS 2010K009), Beijing Jiaotong University, the Beijing Municipal Natural Sceience Foundation (Grant no. 4112048), the Opening Project of the Key Laboratory of Cognitive Radio and Information Processing (Guilin University of Electronic Technology), Ministry of Education (Grant No.: 2011KF01), and the China fundamental education basic research project: Polarization characterization of wireless propagation channel.

References

[1] C.-X. Wang, X. Cheng, and D. I. Laurenson, "Vehicle-to-vehicle channel modeling and measurements: recent advances and future challenges", *IEEE Commun. Mag.*, vol. 47, no. 11, pp. 96–103, Nov. 2009.

[2] J. Karedal, A. Johansson, F. Tufvesson, and A. Molisch, "A measurement-based fading model for wireless personal area networks," *IEEE Trans. Wireless Commun.*, vol. 7, no. 11, pp. 4575–4585, Nov. 2008.

[3] P. Almers, K. Haneda, J. Koivunen, V. M. Kolmonen, A. Molisch, A. Richter, J. Salmi, F. Fufvesson, and P. Vainikainen, "A dynamic multi-link MIMO measurement system for 5.3 GHz," *Proc. 29th URSI Gen. Assem.*, Chicago, USA, Aug. 2008.

[4] L. Ahumada, R. Feick, R. Valenzuela, and C. Morales, "Measurement and characterization of the temporal behavior of fixed wireless links," *IEEE Trans. Veh. Techno.*, vol. 54, no. 6, pp. 1913–1922, Nov. 2005.

[5] L. Jiang, L. Thiele, and V. Jungnickel, "Modeling and measurement of MIMO relay channels," *Proc. VTC'08-Spring*, Singapore, May 2008, pp. 419–423.

[6] 3GPP TR 25.996, "Spatial channel model for multiple input multiple output (MIMO) simulations (Rel. 6)," Sept. 2003.

[7] C.-X. Wang, X. Hong, H. Wu, and W. Xu, "Spatial temporal correlation properties of the 3GPP spatial channel model and the Kronecker MIMO channel model," *EURASIP Journal on Wireless Communications and Networking, Special Issue on Space-Time Channel Modeling for Wireless Communications*, vol. 2007, Article ID 39871, 2007. doi:10.1155/2007/39871.

[8] P. Kyosti *et al.*, "WINNER II channel models," IST-WINNER II D1.1.2, Nov. 2007.

[9] C.-X. Wang, X. Hong, X. Ge, X. Cheng, G. Zhang, and J. Thompson, "Cooperative MIMO channel models: A survey," *IEEE Commun. Mag.*, vol. 48, no. 2, pp. 80–87, Feb. 2010.

[10] C. Oestges, N. Czink, B. Bandemer, P. Castiglione, F. Kaltenberger, and A. Paulraj, "Experimental characterization and modeling of outdoor-to-indoor and indoor-to-indoor distributed channels," *IEEE Trans. Veh. Techno.*, vol. 59, no. 3, pp. 2253–2265, June 2010.

[11] W. Xu, S. A. Zekavat, and H. Tong, "A novel spatially correlated multiuser MIMO channel modeling: Impact of surface roughness," *IEEE Trans. Antennas Propag.*, vol. 57, no. 8, pp. 2429–2438, Aug. 2009.

[12] X. Yin, "Spatial cross-correlation of multilink propagation channels in amplify-and-forward relay systems," *Proc. IWonCMM'10*, Beijing, China, Aug. 2010, pp. 1–5.

[13] X. Cheng, C.-X. Wang, H. Wang, X. Gao, X.-H. You, D. Yuan, B. Ai, Q. Huo, L. Song, and B. Jiao, "Cooperative MIMO channel modeling and multi-link spatial correlation properties," *IEEE Journal on Sel. Areas in Commun.*, vol. 30, no. 2, pp. 388–396, Feb. 2012.

[14] M. Pätzold, C.-X. Wang, and B. O. Hogstad, "Two new sum-of-sinusoids-based methods for the efficient generation of multiple uncorrelated Rayleigh fading waveforms," *IEEE Trans. Wireless Commun.*, vol. 8, no. 6, pp. 3122–3131, Jun. 2009.

[15] C.-X. Wang, D. Yuan, H.-H. Chen, and W. Xu, "An improved deterministic SoS channel simulator for efficient simulation of multiple uncorrelated Rayleigh fading channels," *IEEE Trans. Wireless Commun.*, vol. 7, no. 9, pp. 3307–3311, Sept. 2008.

[16] C.-X. Wang, M. Pätzold, and D. Yuan, "Accurate and efficient simulation of multiple uncorrelated Rayleigh fading waveforms," *IEEE Trans. Wireless Commun.*, vol. 6, no. 3, pp. 833–839, Mar. 2007.

[17] C.-X. Wang, M. Pätzold, and Q. Yao, "Stochastic modeling and simulation of frequency correlated wideband fading channels," *IEEE Trans. Veh. Techno.*, vol. 56, no. 3, pp. 1050–1063, May 2007.

[18] X. Cheng, C.-X. Wang, D. I. Laurenson, S. Salous, and A. V. Vasilakos, "An adaptive geometry-based stochastic model for non-isotropic MIMO mobile-to-mobile channels," *IEEE Trans. Wireless Commun.*, vol. 8, no. 9, pp. 4824–4835, Sep. 2009.

[19] X. Cheng, C.-X. Wang, D. I. Laurenson, S. Salous, and A. V. Vasilakos, "New deterministic and stochastic simulation models for non-isotropic scattering mobile-to-mobile Rayleigh fading channels", *Wireless Commun. and Mobile Computing*, John Wiley & Sons, vol. 11, no. 7, pp. 829–842, July 2011.

[20] N. Czink, B. Bandermer, G. Vazquez-Vilar, A. Paulraj, and L. Jalloul, "July 2008 radio measurement campaign: Measurement documentation," Tech. Rep., COST 2100 TD(08)620, Oct. 2008.

[21] A. Abdi, J. A. Barger, and M. Kaveh, "A parametric model for the distribution of the angle of arrival and the associated correlation function and power spectrum at the mobile station," *IEEE Trans. Veh. Techno.*, vol. 51, no. 3, pp. 425–434, May 2002.